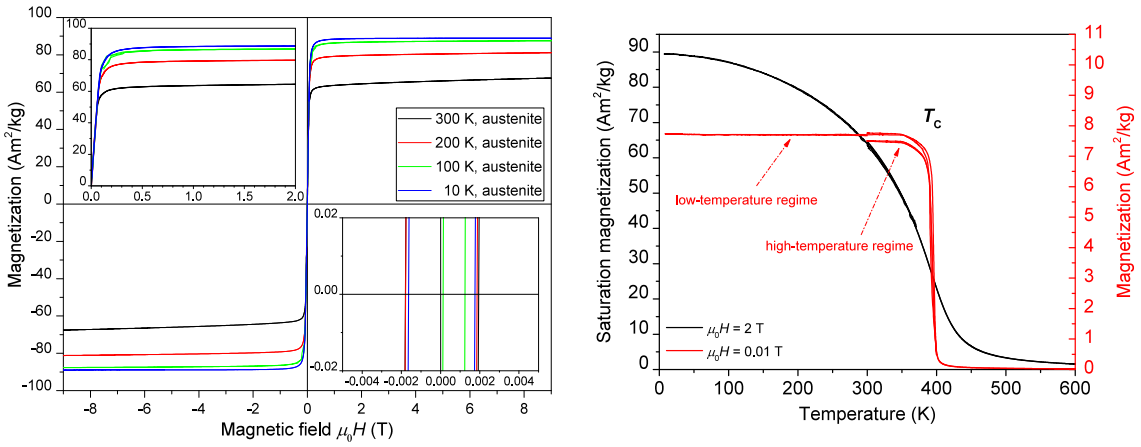

(a) (b)

Figure S1: $(Ni_{45.3}Fe_{5.3})Mn_{23.8}Ga_{25.6}$ (at. %) marked as $Ni_{45}Fe_5$; magnetization curves at several temperatures and the particular phases (a); thermomagnetic curves (b) at low field (0.01 T) and high field (2 T) with Curie temperature (T_C) marked in.

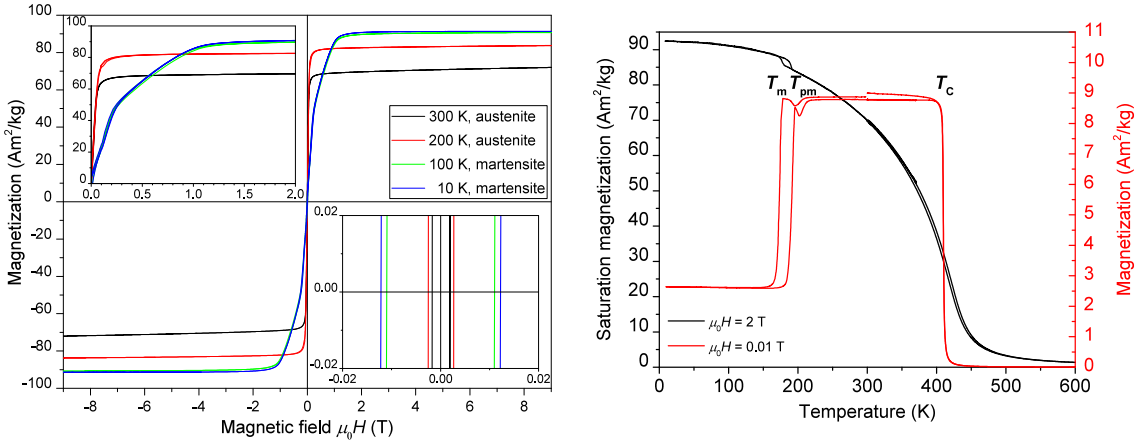

(a) (b)

Figure S2: $Ni_{49.2}(Mn_{20.5}Fe_{5.3})Ga_{25.0}$ (at. %) marked as $Mn_{20}Fe_5$; magnetization curves (a) and thermomagnetic curves (b) with Curie (T_C), premartensitic (T_{pm}) and martensitic transformation (T_m) temperatures marked in.

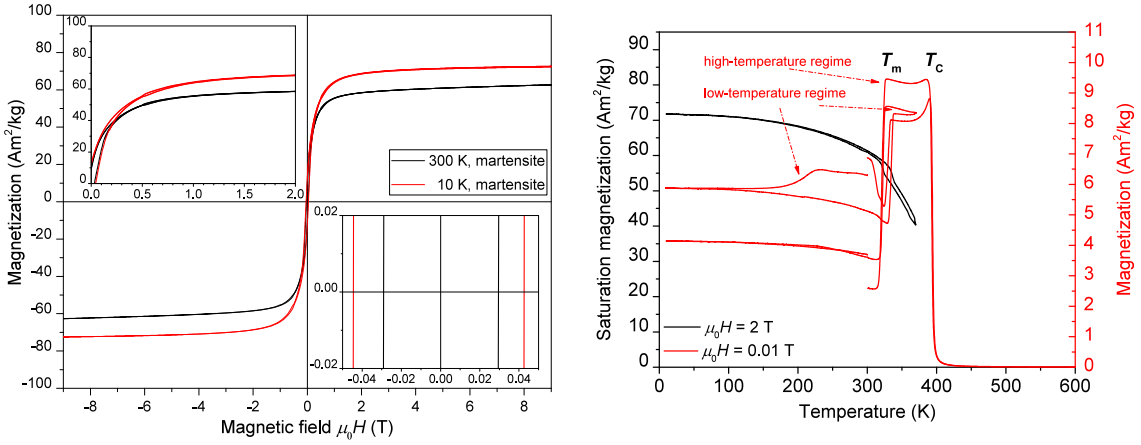

(a) (b)

Figure S3: $Ni_{49.0}Mn_{25.5}(Ga_{20.0}Fe_{5.5})$ (at. %) marked as $Ga_{20}Fe_5$; magnetization curves (a) and thermomagnetic curves (b) with Curie (T_C) and martensitic transformation (T_m) temperatures marked in.

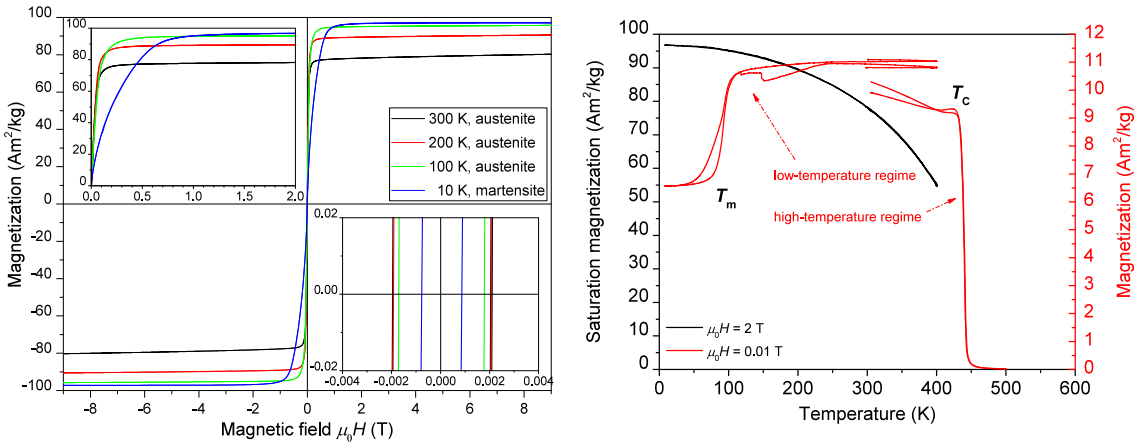

(a) (b)

Figure S4: $(Ni_{44.9}Co_{5.1})Mn_{25.1}Ga_{24.9}$ (at. %) marked as $Ni_{45}Co_5$; magnetization curves (a) and thermomagnetic curves (b) with Curie (T_C) and martensitic transformation (T_m) temperatures marked in.

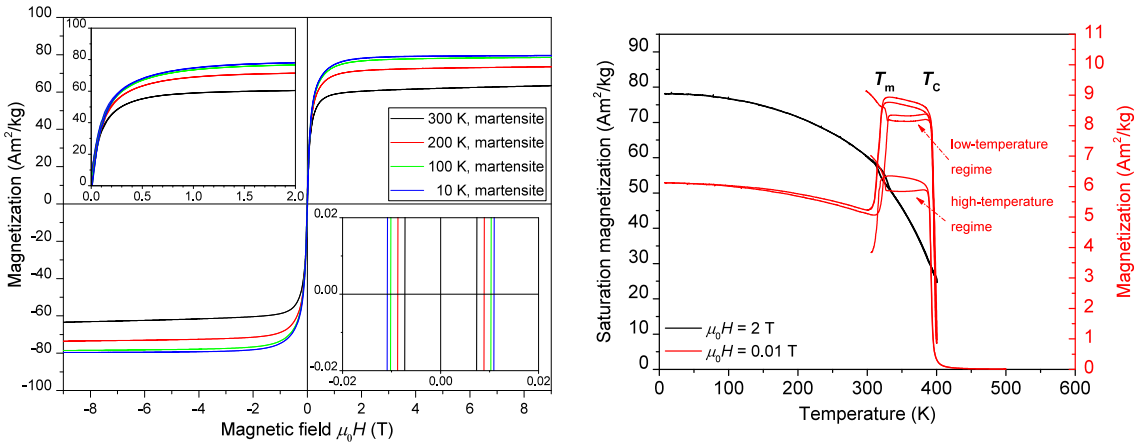

(a) (b)

Figure S5: $Ni_{49.9}(Mn_{20.1}Co_{5.0})Ga_{25.0}$ (at. %) marked as $Mn_{20}Co_5$; magnetization curves (a) and thermomagnetic curves (b) with Curie (T_C) and martensitic transformation (T_m) temperatures marked in.

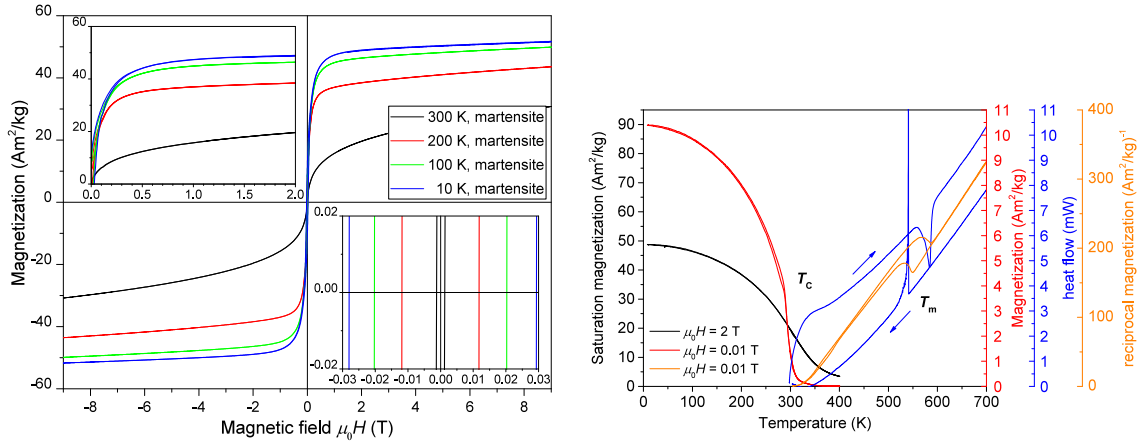

(a) (b)

Figure S6: $Ni_{49.9}Mn_{24.6}(Ga_{20.4}Co_{5.1})$ (at. %) marked as $Ga_{20}Co_5$; magnetization curves (a) and thermomagnetic curves (b) with Curie temperature (T_C) marked in. Differential thermal analysis and reciprocal thermomagnetic measurement were used to detect martensitic transformation temperature (T_m) above Curie temperature.

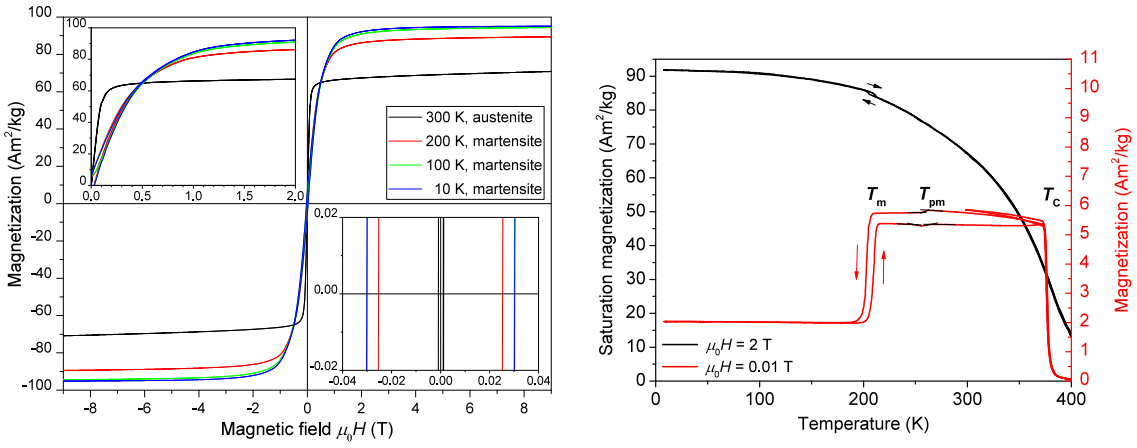

(a) (b)

Figure S7: $(Ni_{45.0}Ni_{5.4})Mn_{24.6}Ga_{25.0}$ (at. %) marked as $Ni_{45}Ni_5$; magnetization curves (a) and thermomagnetic curves (b) with Curie (T_C), premartensitic (T_{pm}) and martensitic transformation (T_m) temperatures marked in.

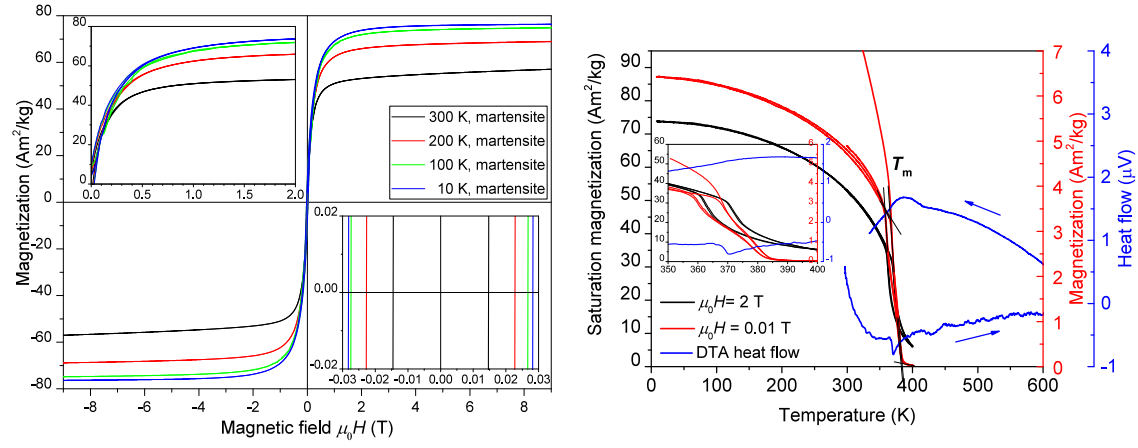

(a) (b)

Figure S8: $Ni_{50.0}(Mn_{20.5}Ni_{4.4})Ga_{25.1}$ (at. %) marked as $Mn_{20}Ni_5$; magnetization curves (a) and thermomagnetic curves (b) with Curie (T_C) and martensitic transformation (T_m) temperatures marked in. Differential thermal analysis (DTA) was used to confirm the appearance of martensitic transformation (T_m) temperature.

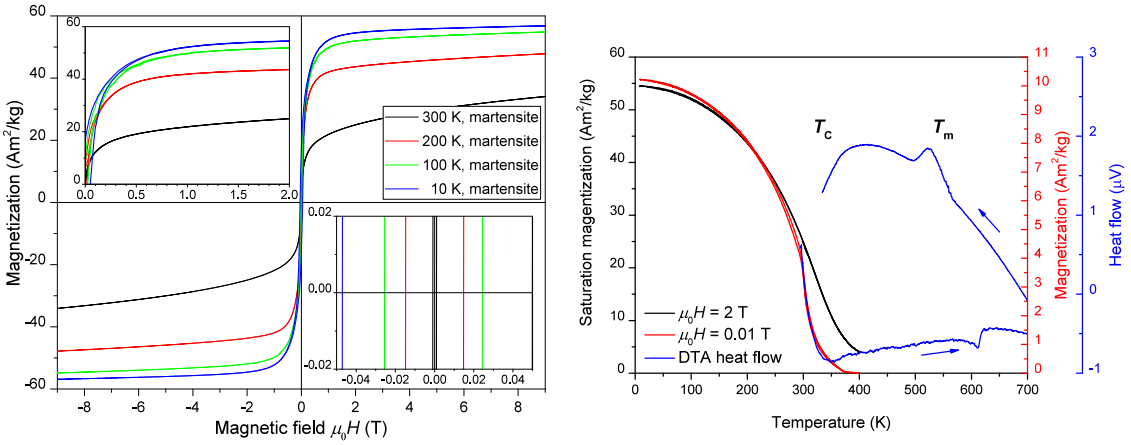

(a) (b)

Figure S9: $Ni_{50.0}Mn_{25.4}(Ga_{20.3}Ni_{4.3})$ (at. %) marked as $Ga_{20}Ni_5$; magnetization curves (a) and thermomagnetic curves (b) with Curie (T_C) and martensitic transformation (T_m) temperatures marked in. Differential thermal analysis (DTA) was used to determine the appearance of martensitic transformation (T_m) temperature.

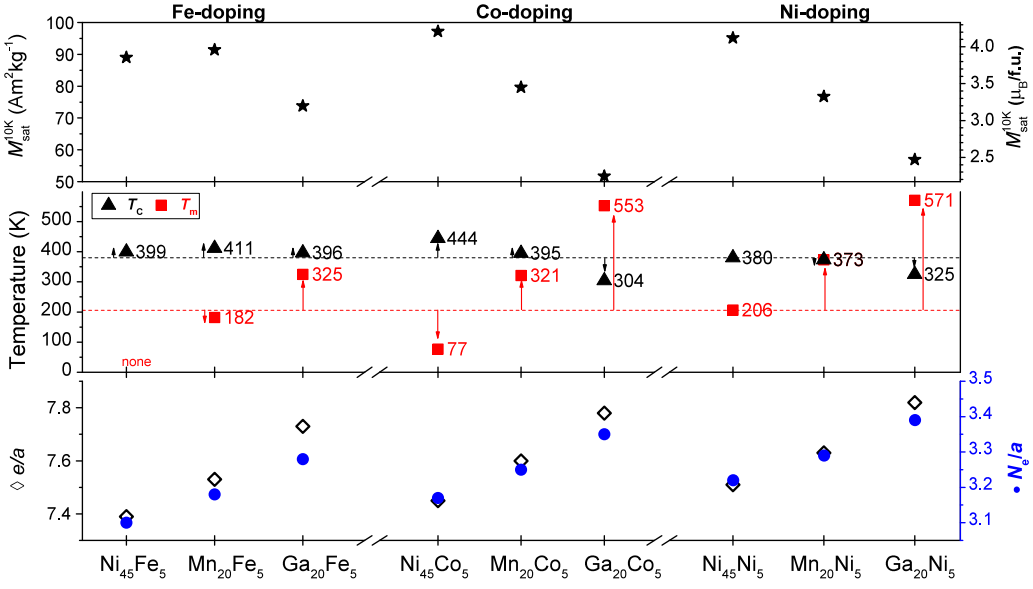

Figure S10: Transition temperatures dependence on composition. The full alloys compositions are in each particular Figure. The relative shift compared to stoichiometry alloy $Ni_{45}Ni_5$ is marked by arrows. The transformation temperatures of stoichiometry alloy are marked by dashed lines. In addition, saturation magnetization $M_{\mathrm{sat}}^{10\mathrm{K}}$, *e/a* and N_e/a parameters are shown for comparison.

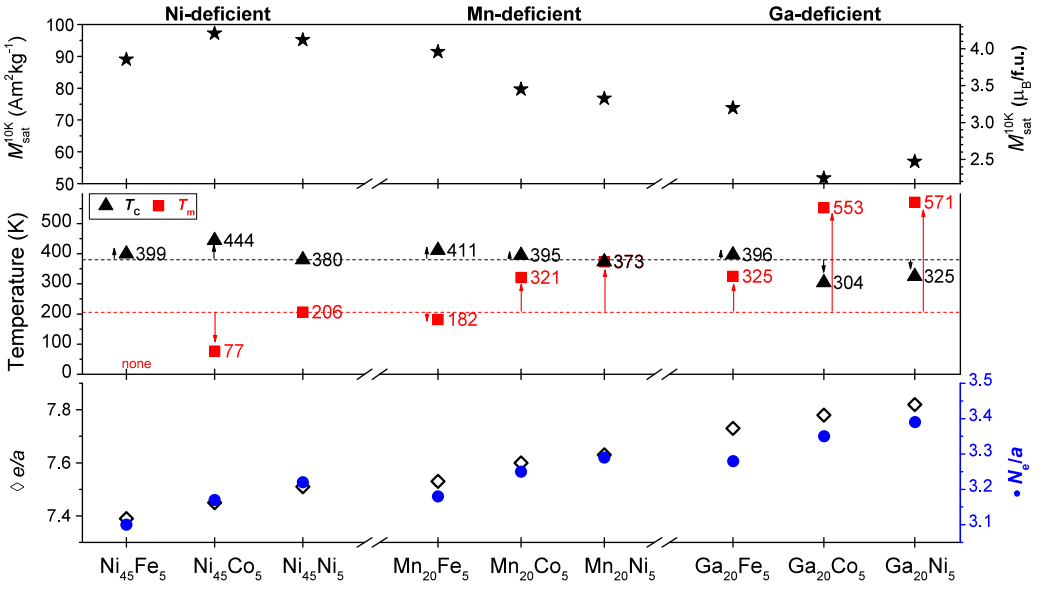

Figure S11: Transition temperatures dependences on composition rearranged according to a doping site. In addition, saturation magnetization $M_{\mathrm{sat}}^{10\mathrm{K}}$ and *e/a* and N_e/a parameters are plotted for comparison. The dashed lines mark transition temperatures of the stoichiometric compound and the arrows emphasize a temperature deviation from it.

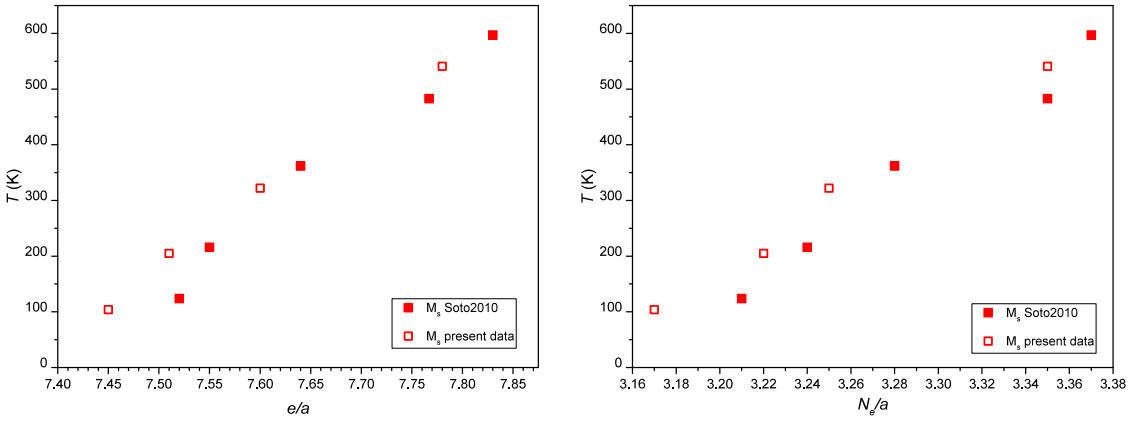

Figure S12: Comparison of martensitic start temperatures (M_s) of Co-doped and stoichiometric alloys with respect to valence electrons per atom (*e/a*) and non-bonding valence electrons N_e/a. The full citation of the compared paper is provided in the paper [15].

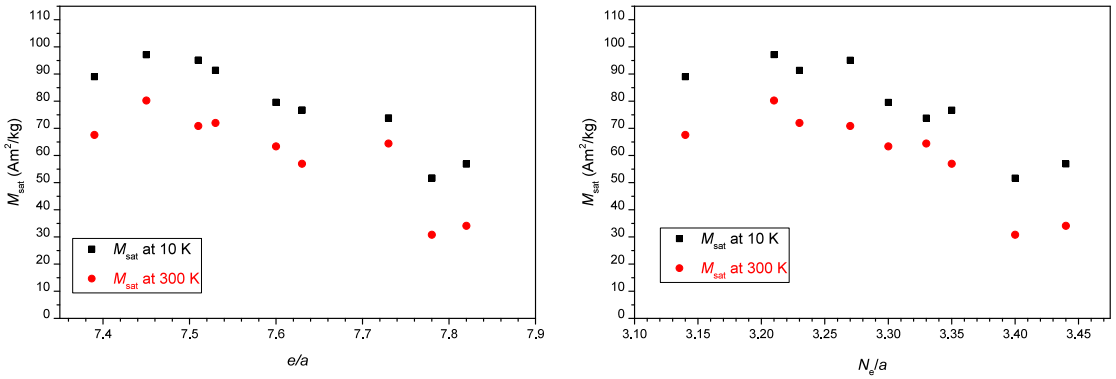

(a) (b)

Figure S13: Saturation magnetization (M_{sat}) at 10 and 300 K measured at 9 T with respect to valence electrons per atom (e/a) and non-bonding valence electrons N_e/a.

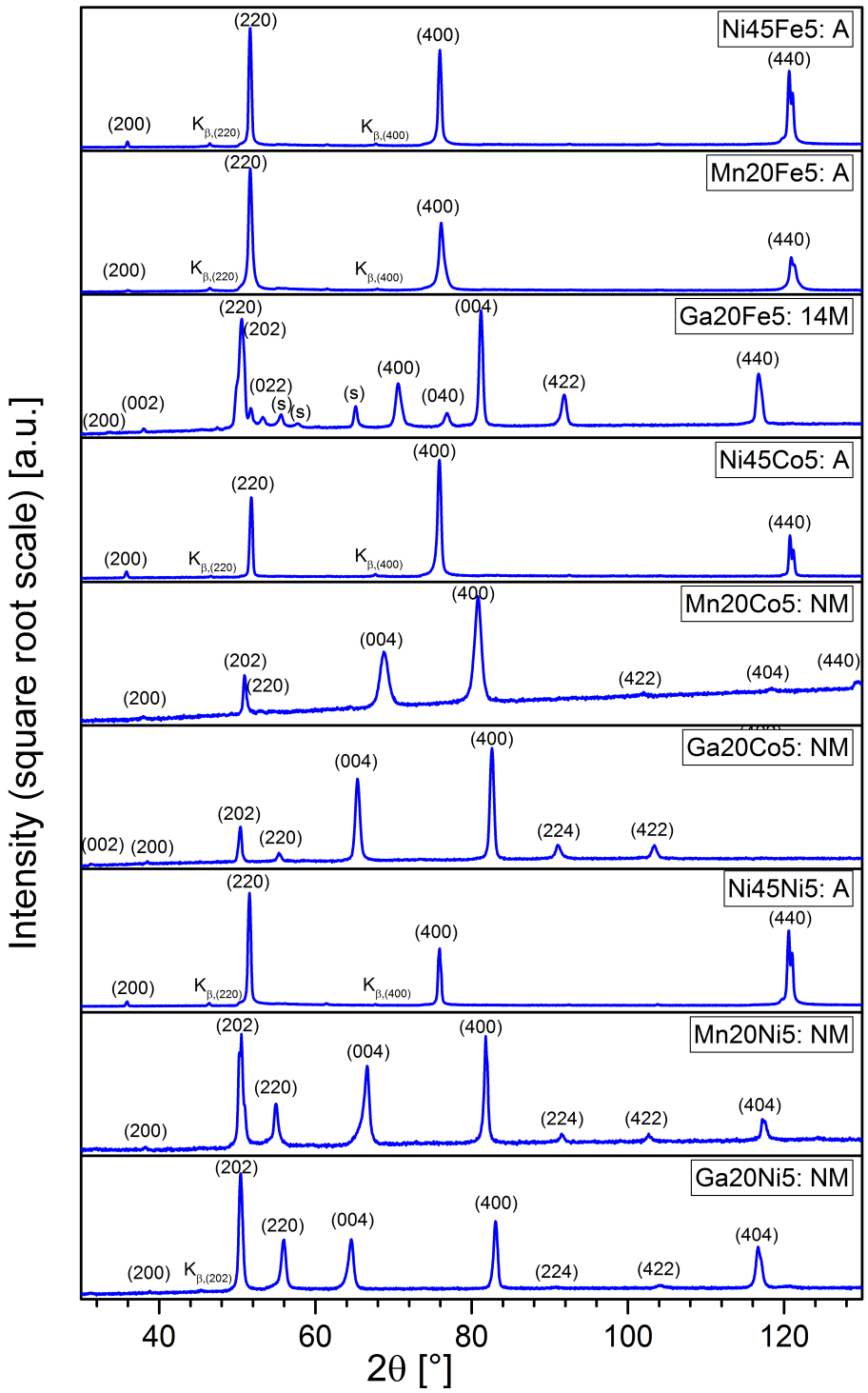

Figure S14: X-ray diffraction patterns, strong peaks indexed. Each pattern represents a sum of at least three scans collected at different sample orientations (suggested by the pole figures) due to their oligocrystalline nature. Strong satellite reflections of the 14M modulated martensite are marked *(s)*. Strong K_β lines of the X-ray tube spectrum noticeable in some scans are also marked to prevent confusion.